

Model Predictive Control with Visibility Graphs for Humanoid Path Planning and Tracking Against Adversarial Opponents

Ruochen Hou¹, Gabriel I. Fernandez¹, Mingzhang Zhu¹, and Dennis W. Hong¹

Abstract—In this paper we detail the methods used for obstacle avoidance, path planning, and trajectory tracking that helped us win the adult-sized, autonomous humanoid soccer league in RoboCup 2024. Our team was undefeated for all seated matches and scored 45 goals over 6 games, winning the championship game 6 to 1. During the competition, a major challenge for collision avoidance was the measurement noise coming from bipedal locomotion and a limited field of view (FOV). Furthermore, obstacles would sporadically jump in and out of our planned trajectory. At times our estimator would place our robot inside a hard constraint. Any planner in this competition must also be computationally efficient enough to re-plan and react in real time. This motivated our approach to trajectory generation and tracking. In many scenarios long-term and short-term planning is needed. To efficiently find a long-term general path that avoids all obstacles we developed DAVG (Dynamic Augmented Visibility Graphs). DAVG focuses on essential path planning by setting certain regions to be active based on obstacles and the desired goal pose. By augmenting the states in the graph, turning angles are considered, which is crucial for a large soccer playing robot as turning may be more costly. A trajectory is formed by linearly interpolating between discrete points generated by DAVG. A modified version of model predictive control (MPC) is used to then track this trajectory called cf-MPC (Collision-Free MPC). This ensures short-term planning. Without having to switch formulations cf-MPC takes into account the robot dynamics and collision free constraints. Without a hard switch the control input can smoothly transition in cases where the noise places our robot inside a constraint boundary. The nonlinear formulation runs at approximately 120 Hz, while the quadratic version achieves around 400 Hz.

I. INTRODUCTION

Finding a collision-free path is essential for any robot operating in a complex environment. In RoboCup 2024 adult-sized, autonomous humanoid soccer competition, 2 human referees, 4 robot handlers and 4 robots are constantly moving on a 14 m by 9 m field of which at times feels much smaller since everyone crowds the ball. This requires our robot, ARTEMIS, not only to plan obstacle-free paths in real time but also to re-plan and track effectively in spite of the vast amounts of noise, e.g., humans jumping in and out of frame. Our path planning and tracking process is shown in Fig. 1. Given an initial and final pose, the path planner finds the optimal path while avoiding obstacles using a modified version of visibility graphs called dynamic augmented visibility graphs (DAVG). Linear interpolation is then used to fill in the points with a time stamp. Finally, a

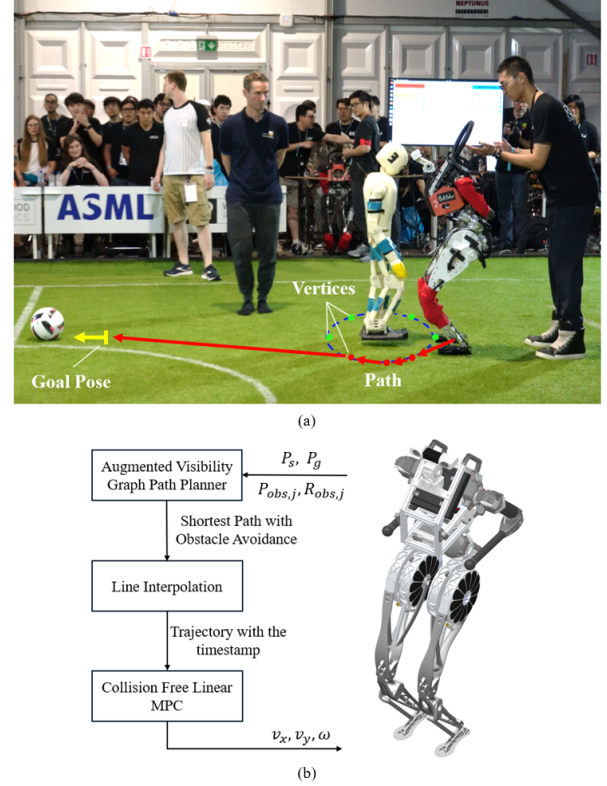


Fig. 1: *Top* figure shows a situation where our robot, ARTEMIS, in red is trying to avoid the opponent in blue to get to the ball during the championship match in RoboCup 2024. There are many situations like this or even worse when trying to reach the ball. *Bottom* figure gives an overview of our entire framework for trajectory generation and tracking. P_s and P_g represent the starting pose and goal pose, respectively. $P_{obs,j}$ and $R_{obs,j}$ represent the position and radius of obstacles, respectively.

modified version of Model Predictive Control (MPC), called Collision-Free MPC (cf-MPC), generates a control signal that ensures smooth, collision-free motion while considering the robot's dynamics. This planner played a big role in helping us score over 45 goals in 6 seated games in RoboCup 2024 and ultimately secure the championship title [1].

There are numerous methods for path planning: learning based methods [2]–[5], nonlinear optimization methods [6]–[8], control lyapunov function (CLF) and control barrier function (CBF) methods [9]–[14], heuristic methods like potential fields [15]–[19], reachability methods [20], [21], convex optimization with Bézier curves in Graphs of Convex Sets (GCS) [22], [23], rapidly-exploring random trees (RRT) [24], [25], search based algorithms like A*[26].

Path planning for a 35+ kg humanoid robot capable of running at 2 m/s must efficiently re-plan in a dynamic and complex environment, particularly when penalties ap-

This paper has been accepted to IEEE International Conference on Robotics and Automation (ICRA) 2025. ¹Robotics and Mechanisms Laboratory (RoMeLa), Department of Mechanical and Aerospace Engineering, University of California, Los Angeles, CA 90095, USA. {houruochen, gabriel1808, normanzmz, dennishong}@ucla.edu

ply for collisions with opponents. Moreover, computational efficiency is critical due to the hardware constraints and limited processing resources available on a humanoid robot. To address these challenges, we chose a graph-based method, as it is computationally efficient and avoids local minima, ensuring a reliable long-term trajectory from start to finish.

Graphs have many different representations: uniform grids, log-polar grid which is non-uniform and denser around robots and obstacles [26], [27], vertices of recursively divided blocks by quadtree [28], visibility graphs where the nodes are the vertices of the obstacles [29]–[32] or waypoints of suboptimal paths [28]. Our proposed approach uses a type of visibility graph that chooses the vertices of the obstacles to be nodes. The shortest path in Euclidean space would be a straight line or along an edge of a convex obstacle. In our case we augment the states to account for turning since that slows our robot down. Our proposed method, DAVG, is further enhanced by using active regions and obstacles such that the entire graph does not need to be searched.

DAVG generates discrete points which we then interpolate between by assigning a time stamp to each point in the path. Since turning takes a longer than building momentum and running straight, we use linear interpolation, which is C_0 continuous. This also maintains the shortest path property in Euclidean space. A potential added benefit is that when re-planning does occur the swings in changes between updated paths are reduced because of the lack of curvature.

MPC is popular for trajectory tracking [33]. It can deal with nonlinear models and complex constraints directly without fine detailed modelling. In fact, for wheeled mobile robot models, which is nonholonomic, it is impossible to stabilize around the equilibrium point using smooth time-invariant feedback control [34]–[36]. In [35], to speed up the MPC, the authors described an explicit MPC where the optimal solution is calculated off-line and then used in the form of a look-up table. In [36], a nonlinear MPC (NMPC) with nonlinear obstacle avoidance constraints is introduced. It switches between tracking mode and obstacle avoidance mode using different objective functions. Our proposed method, cf-MPC, does not use switching for collision avoidance. cf-MPC has one problem formulation which allows for smoother transitions when balancing obstacle avoidance and robot dynamics. This played a very crucial role during RoboCup when obstacles flashed in and out of our path and constraints. We can also linearize and simplify the constraints, and the formulation becomes a linear MPC (LMPC) which is a quadratic program (QP) problem, i.e., an efficiently solved problem.

The following is a summary of contributions in this paper:

- 1) Introduce DAVG which is capable of finding the shortest path efficiently while accounting for turning angles,
- 2) Introduce cf-MPC which balances obstacles avoidance and robot dynamics into a single formulation in QP,
- 3) Demonstrate its capabilities on hardware and in competition where we won RoboCup 2024.

The article is organized as follows: in Section II DAVG is detailed, in Section III cf-MPC is covered, and in Section IV

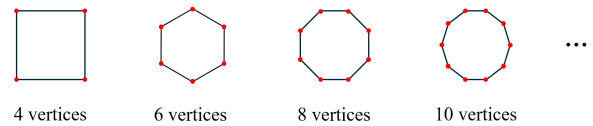


Fig. 2: Regular polygon representation of obstacles.

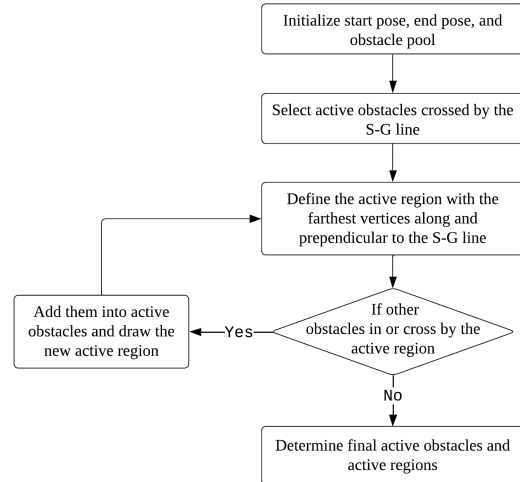


Fig. 3: Process for selecting active obstacles and active regions.

corresponding experiments and results are shown.

II. PATH PLANNING BY DAVG

Visibility graphs proposed by Lozano-Pérez and Wesley [29] is a classical method of finding the shortest path of a point among polygonal obstacles. In our case, each obstacle (robot or person) is represented by a regular polygon 2. There are multiple methods to solve a visibility graph like A* [37], Dijkstra's algorithm [38], [39], or linear programming[40].

A. Preprocessing

For complex environments, there may be many obstacles. Taking all vertices into account would be computational burdensome, and in fact some obstacles will not influence the optimal path. To make the computational load more efficient, we only select necessary obstacles. Dynamic visibility graphs (DVG) by Huang and Chung [32] introduced a method to select active regions which contain only the necessary vertices and remove unnecessary ones. However, their method is complex when comparing the longest inner path and shortest outer path. In DAVG, we simplify this process. The preprocess procedures are shown in Fig. 3, and an example is given in Fig. 4. We define the straight line connecting the start and ending points as S-G line. A straight line is optimal in Euclidean space. A choice of a different space would result in a different optimal path absence of obstacles. Firstly, our algorithm finds the obstacles that intersect the S-G line, which forms the first active obstacles. These obstacles might influence the optimal trajectory. Then we find the farthest vertices along the S-G line and perpendicular to the S-G line. These define the length and width of the active region, which covers all the active obstacles. Then we check

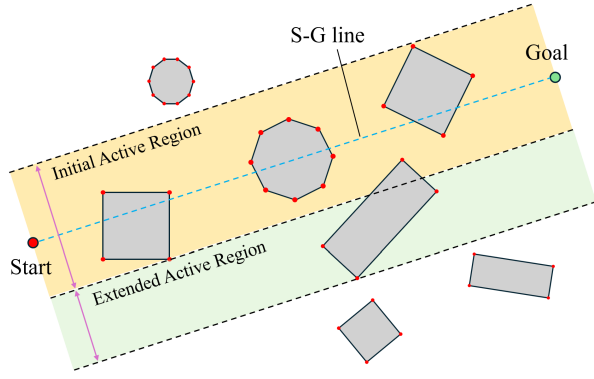


Fig. 4: Illustration of selecting active region procedure.

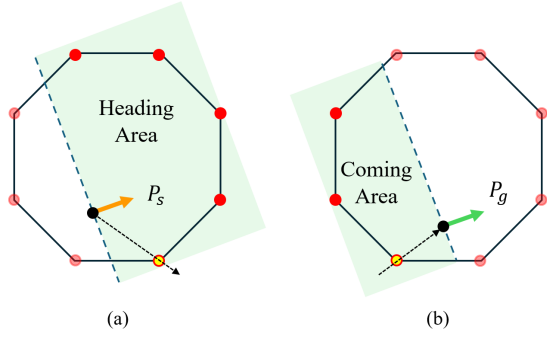


Fig. 5: How to define the edge when the starting point or ending point is covered by an obstacle.

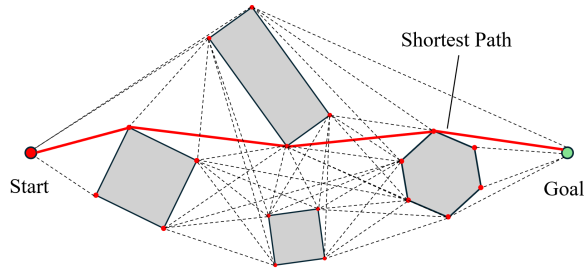


Fig. 6: Finding the shortest path by our visibility graph called DAVG.

if there are other obstacles intersecting the active region. If there are, add these obstacles to the active obstacle since they might influence the optimal path and calculate the new active region. Repeat this until no obstacles intersect the active region, meaning that the obstacles outside of active region will not influence the optimal path.

B. Shortest Path by Visibility Graph

First we construct a visibility graph to find the shortest path that minimizes Euclidean distance. The nodes include the starting point S , goal point G and vertices of the active obstacles V_i which are not covered by other obstacles. There is an edge between two nodes if the edge does not have any intersections with obstacles. The weight of the edge connecting two nodes is the Euclidean distance. All such edges are generated.

If the starting point or the ending point is covered by an obstacle, they will not have an edge connecting them,

Algorithm 1 Algorithm to Construct a Visibility Graph

```

1: Initialize the Graph:
2: Let  $VG = (V, E)$ , where  $V$  is the set of all nodes (start
   point  $S$ , goal point  $G$ , and obstacle vertices  $V_i$ ), and  $E$ 
   is initially an empty set of edges.
3: Remove invisible nodes:
4: for all nodes in  $V$  do
5:   if node is covered by some obstacle then
6:     Remove it from the set  $V$ .
7:   end if
8: end for
9: Define Edges by Looping Through All Pairs of Nodes:
10: for all pairs of nodes  $(V_i, V_j) \in V$  do
11:   Check Visibility:
12:   Draw a line segment between  $V_i$  and  $V_j$ .
13:   if line segment does not intersect any obstacle then
14:     Add edge  $(V_i, V_j)$  to  $E$  with distance weight.
15:   end if
16: end for
17: Define the Edge if  $P_s$  or  $P_g$  in Obstacle:
18: if  $P_s$  or  $P_g$  is in obstacle then
19:   Choose the leaving vertex on obstacle:
20:   if  $P_s$  then
21:     The vertex should be in the going direction.
22:   else
23:     The vertex should be in the entering direction.
24:   end if
25:   Choose the closest vertex.
26:   Define edge between chosen vertex and  $P_s$  or  $P_g$ .
27: end if

```

and they are also not added to the node set V . We need to define vertices to go out of the obstacle in this case so that we can keep moving along similar directions. For starting points, the vertex should be in the *heading* direction. For an obstructed goal point, the vertices should be in the *coming* direction. If we are in the obstacles constraint, we want the path to go out of the obstacle as fast as possible as depicted in Fig. 5. Therefore, the closest one is chosen. Finally, an edge exists between the chosen vertex and the starting point or the ending point. Fig. 6 illustrates an example of finding the shortest path on such a graph.

C. Shortest Path with Turning Angle

A visibility graph does not inherently account for constraints like minimizing the turning angles along the path. The shortest path found by a visibility graph might have sharp turns, especially, around obstacle corners, since it connects visible vertices with straight lines. For humanoid robots and many other systems turning is time-consuming. Therefore, it is preferable to take the turning angle into consideration when constructing these graphs. One way to achieve this is to augment the states. The current weight of the edge between two states depends on both the Euclidean distance and turning angle. We call this modified graph an augmented visibility graph (AVG). Fig. 7 depicts an example by which the path is altered by using AVG for turning angles.

Algorithm 2 Augmented Visibility Graph

```

1: Initialize the Graph:
2: Let  $AVG = (\hat{V}, \hat{E})$ , where  $\hat{V}$  is the set of all combined
   state nodes, and  $\hat{E}$  is initially an empty set of edges.
3: Construct the normal Visibility Graph  $VG = (V, E)$ 
   as described in Algorithm 1.
4: Define the Combined State:
5: for all edges  $(V_i, V_j) \in E$  do
6:   Represent combined state as  $\hat{V}_{ij} = (V_i, V_j)$ , where:
7:    $V_i$  represents the past vertex.
8:    $V_j$  represents the current vertex.
9:   Add  $\hat{V}_{ij}$  to the set  $\hat{V}$ .
10: end for
11: Add starting state  $\hat{S}$  and goal state  $\hat{G}$  to  $\hat{V}$ .
12: Define Edges and Weights with Combined States:
13: for all nodes  $\hat{V}_{ij}$  and  $\hat{V}_{jk}$   $\in \hat{V}$  do
14:   if an edge exists between  $V_i$  and  $V_j$  then
15:     Add edge  $\hat{E}_{ijk}$  to  $\hat{E}$ , connecting  $\hat{V}_{ij}$  and  $\hat{V}_{jk}$ .
16:     Weight of  $\hat{E}_{ijk}$  combines Euclidean distance  $E_{jk}$ 
17:     and turning angle from  $E_{ij}$  to  $E_{jk}$ .
18:   end if
19: end for

```

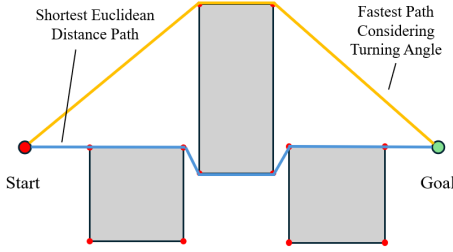


Fig. 7: How the augmented visibility graph gives a different path by augmenting the state with a weight determined by the turning angle.

Turning angles are added in as additional weights on the edges of the graph. For humanoid robots, turning can be slow, and, therefore, the outer path is chosen, though longer, reduces the amount of turning. The combination of active regions and augmented edges defines DAVG.

III. TRAJECTORY TRACKING

Interpolating the results from DAVG, we get a trajectory which avoids obstacles. This section shows how to track that trajectory with an MPC. Note that even though we can guarantee that the trajectory from DAVG will avoid obstacles in theory, the robot can still collide with obstacles if it cannot track its trajectory well. In some cases the robot cannot properly track its trajectory due to its dynamic and physical limitations, e.g., speed and acceleration limits. Therefore, we introduce a collision free constraint to the MPC to help the robot avoid obstacles. The constraint can be relaxed to ensure a feasible solutions while trying to avoid the obstacle. This provides a method for short-term planning.

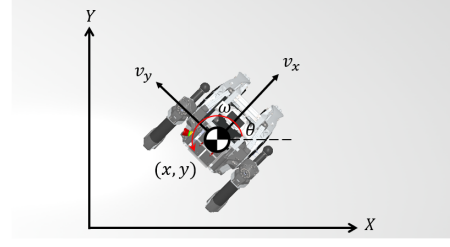


Fig. 8: Coordinate system for our humanoid robot.

A. Dynamic Model

The 2D pose on the field is $\mathbf{p} := [x \ y \ \theta]^T$, where $x \in \mathbb{R}, y \in \mathbb{R}$ is the position and $\theta \in (-\pi, \pi]$ is the orientation, shown in Fig. 8. For a humanoid, it is capable of moving both forward and sideways. In the analysis below, we are using the humanoid model. However, in fact, the ability for a humanoid robot to move sideways might be poor. Therefore, it is acceptable to use a model for mobile robots for simplicity. The discretized model we used is as follows:

$$\begin{bmatrix} x_{k+1} \\ y_{k+1} \\ \theta_{k+1} \end{bmatrix} = \begin{bmatrix} x_k \\ y_k \\ \theta_k \end{bmatrix} + \begin{bmatrix} \cos(\theta_k) & -\sin(\theta_k) & 0 \\ \sin(\theta_k) & \cos(\theta_k) & 0 \\ 0 & 0 & 1 \end{bmatrix} \begin{bmatrix} v_x \\ v_y \\ \omega \end{bmatrix} dt$$

where dt is the time step. Define the state X and control input u as : $\mathbf{X}_k := [x_k \ y_k \ \theta_k]^T$ and $\mathbf{u}_k := [v_{xk} \ v_{yk} \ \omega_k]^T$. The system is as follows:

$$X_{k+1} = f_d(X_k, u_k)$$

B. Nonlinear Model Predictive Control

In NMPC, we predict the next N steps, and the objective function is formulated to track its reference trajectory. Considering the discrete dynamics of a humanoid robot, the objective function for the NMPC is as follows:

$$J_0 = \sum_{i=1}^N (X_i - X_{r,i})^T Q (X_i - X_{r,i}) + \sum_{i=0}^{N-1} u_i^T R u_i$$

where $X_{r,i}$ is the reference state at time step i . $Q \in \mathbb{R}^{n \times n}$ is a weight matrix, and $R \in \mathbb{R}^{m \times m}$ is a weight matrix. The reference trajectory follows:

$$X_{r,k+1} = f_d(X_{r,k}, u_{r,k})$$

The initial point is X_0 , and its dynamic constraint is as follows:

$$x_{i+1} = f_d(x_i, u_i), \quad i = 0, \dots, N-1$$

As we define a circular region that we do not want the trajectory to violate, the collision free constraint is as follows:

$$(x_i - x_{\text{obs},j})^2 + (y_i - y_{\text{obs},j})^2 \geq R^2, \quad \forall_{j=1, \dots, k}^{i=1, \dots, N}$$

We can add a positive slack variable $\delta_j \in \mathbb{R}^+$ to relax the hard collision free constraint to make sure that the problem is feasible.

$$(x_i - x_{\text{obs},j})^2 + (y_i - y_{\text{obs},j})^2 + \delta_j \geq R^2, \quad \forall_{j=1, \dots, k}^{i=1, \dots, N}$$

$$\delta_j \geq 0$$

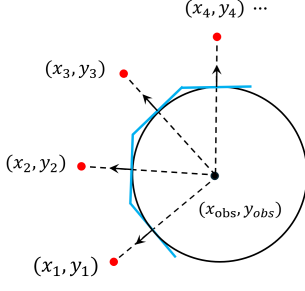


Fig. 9: Linearization of collision free constraints.

The objective function becomes:

$$J = J_0 + \rho \sum_{j=1}^k \delta_j^2 \quad (1)$$

where ρ is the weight on the collision free constraint. Larger ρ makes the constraint stricter. We can also add a speed constraint:

$$\begin{bmatrix} v_{xmin} \\ v_{ymin} \\ \omega_{min} \end{bmatrix} \leq \begin{bmatrix} v_{xk} \\ v_{yk} \\ \omega_k \end{bmatrix} \leq \begin{bmatrix} v_{xmax} \\ v_{ymax} \\ \omega_{max} \end{bmatrix} \quad (2)$$

This is a summary of the NMPC formulation:

$$\begin{aligned} \min_{\substack{X_{1:N} \\ u_{0:N-1}}} J \text{ from Eq. (1)} \\ \text{s.t. } X_{r,k+1} &= f_d(X_{r,k}, u_{r,k}) \\ (x_k - x_{obs,j})^2 + (y_k - y_{obs,j})^2 + \delta_j &\geq R^2 \\ \delta_j &\geq 0 \\ \text{Speed constraint from Eq. (2)} \end{aligned}$$

C. Linear Model Predictive Control

To make the optimization faster, the dynamic model can be linearized around the trajectory. We compute the Jacobian matrices of the nonlinear discrete-time dynamics with respect to the state and input at the current linearization point:

$$A_k = \left. \frac{\partial f_d(X, u)}{\partial X} \right|_{\substack{X=X_{r,k} \\ u=u_{r,k}}} \quad B_k = \left. \frac{\partial f_d(X, u)}{\partial u} \right|_{\substack{X=X_{r,k} \\ u=u_{r,k}}}$$

where: $A_k \in \mathbb{R}^{n \times n}$ is the Jacobian matrix with respect to the state at time step k , and $B_k \in \mathbb{R}^{n \times m}$ is the Jacobian matrix with respect to the input at time step k . Therefore, the dynamic constraints is as follows:

$$X_{k+1} = X_k + A_k(X_k - X_{r,k}) + B_k(u_k - u_{r,k})$$

Additionally, the collision free constraint can also be simplified by linear constraints. The obstacle circle can be replaced by its tangent plane as shown in Fig. 9. Define $V_{k,j} = \begin{bmatrix} x_{r,k} - x_{obs,j} \\ y_{r,k} - y_{obs,j} \end{bmatrix}$, then the collision free constraint becomes:

$$\begin{bmatrix} x_k - x_{obs,j} & y_k - y_{obs,j} \end{bmatrix} V_{k,j} \geq \|V_{k,j}\| (R_{obs,j} - \delta_j)$$

It is a linear constraint, where $R_{obs,j}$ is the radius of

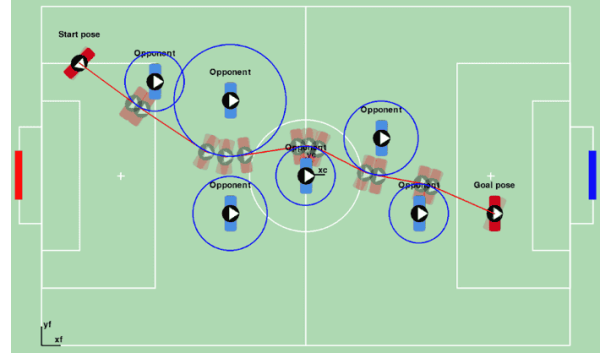


Fig. 10: Diagram of the optimal path of DAVG.

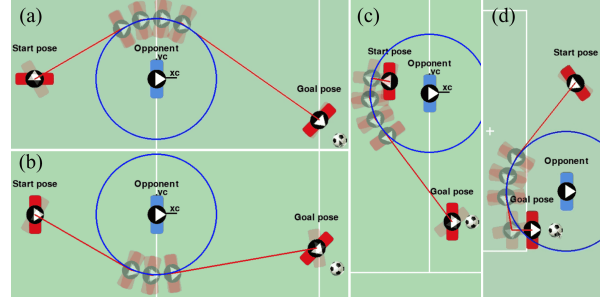


Fig. 11: Diagram of specific cases of DAVG: (a) and (b) show how the turning angle affects the choice of the optimal path in simulation; (c) is an example of finding a vertex to exit an obstacle from an internal starting point; and (d) is an example of finding a vertex to exit an obstacle from an internal ending point.

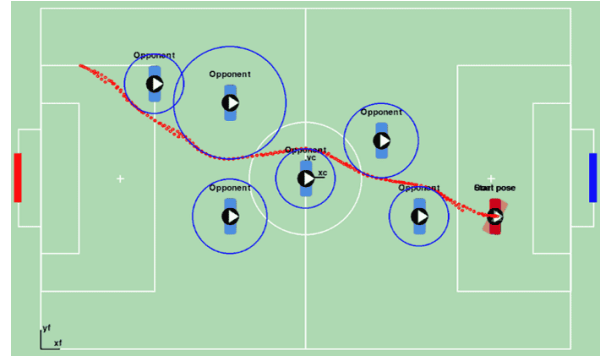


Fig. 12: Diagram of our linear cf-MPC tracking the calculated path in 10.

obstacle j , and δ_j is a slack variable for obstacle j to relax the constraint and guarantee feasibility. Therefore, in summary, the LMPC can be formulated as a QP problem in the following:

$$\begin{aligned} \min_{\substack{X_{1:N} \\ u_{0:N-1}}} J \text{ cost from Eq. (1)} \\ \text{s.t. } X_{r,k+1} &= f_d(X_{r,k}, u_{r,k}) \\ \begin{bmatrix} x_k - x_{obs,j} & y_k - y_{obs,j} \end{bmatrix} V_{k,j} &\geq \|V_{k,j}\| (R_{obs,j} - \delta_j) \\ \delta_j &\geq 0 \\ \text{Speed constraint from Eq. (2)} \end{aligned}$$

IV. RESULTS

In this section, we present both the simulation and hardware implementation of our proposed path planning and trajectory tracking method. We also encourage readers to view

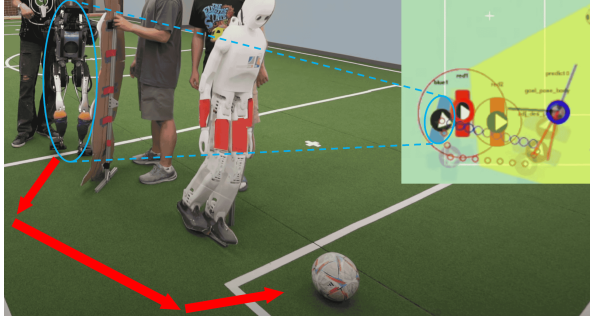


Fig. 13: Field test on ARTEMIS with the path visualization when obstacles flash suddenly into the path. Red dots on the visualizer represent the new path while blue dots represent the old path.

the online competition videos to evaluate our performance. For the simulation, we modeled a soccer field in Python to validate our approach. The nonlinear problem was solved using SNOPT, and the linear problem with Gurobi. All code was executed on an HP Elite Mini 800 G9, equipped with an Intel Core i7-12700T processor and an Nvidia GeForce RTX 3050 Ti 4GB GPU.

A. Path Planning Simulation

First, we present a simulation result of the optimal path found by our DAVG method, with 6 obstacles of varying sizes present on the field, as shown in the Fig. 10. Each obstacle is represented by a polygon with 18 sides. The red poses with higher transparency around obstacles represents vertices on the path.

We then tested some specific properties of the DAVG method. Fig. 11 (a) and (b) shows how the augmented visibility graph generates different paths by giving different starting angles. Fig. 11 (c) and (d) demonstrates our method successfully finding optimal vertices to exit when the starting or ending point is covered by an obstacle.

B. MPC Simulation

We validated the LMPC performance before implementing it on hardware. Ten-step horizons are predicted at each time step in our LMPC, with each time step fixed at 0.25s. The actual control output is shown in Fig. 12. It demonstrates good tracking performance. This result highlights the effectiveness of our framework and its readiness for implementation on the actual hardware platform for competition.

C. Hardware Implementation

We have also demonstrated the feasibility of our proposed control framework through hardware experiments using our humanoid robot, ARTEMIS. The robot's location is determined using the localization methods we have proposed [41]. Fig. 13 shows a snapshot of the experiment where obstacles were suddenly placed in front of ARTEMIS. The adjusted path, even when ARTEMIS was already within the circular constraint region of the obstacle, illustrates the framework's capability to avoid sudden obstacles. Fig. 14 shows snapshots of ARTEMIS successfully maneuvering around an opponent moving along a straight path to the soccer ball, retrieving it, and clearing it from the penalty area for defensive play.



Fig. 14: ARTEMIS successfully bypasses the opponent robot in the competition and retrieves the ball.

D. Solving Time

The DAVG solving time is mainly influenced by the number of obstacles and the number of arcs for each polygon. Table I shows the average solving time of DAVG.

TABLE I: DAVG Solving Time

N_obs	2		4		6		8	
N_arc	4	10	4	10	4	10	4	10
(ms)	0.33	1.1	0.53	2.1	0.77	4.3	1.41	8.0

The MPC solving time is mainly influenced by the prediction horizon. Table II shows the average solving time of LMPC and NMPC with two obstacles in the way.

TABLE II: LMPC and NMPC average solving time

N_step	5	10	15	20
LMPC (ms)	0.65	0.88	1.1	1.4
NMPC (ms)	4.2	15.8	40.6	84.6

In the competition, the path planning and tracking process runs at 80–100 Hz using NMPC and around 400 Hz using LMPC, while also handling other computationally intensive tasks such as vision, localization, locomotion, and high-level decision-making on the same computer.

V. CONCLUSION

In this paper, we proposed DAVG which is capable of finding the shortest path efficiently while taking turning angle into account by augmenting states, since for our humanoid robot turning is more difficult and time consuming. To track this path we proposed cf-MPC which balances avoiding obstacles and robot dynamics into a single formulation as opposed to other switching methods. This provides for a smooth transition between tracking and obstacle avoidance which is necessary in such a noisy environment. The combination of both DAVG and cf-MPC allow for a good combination of long-term and short-term planning while maintaining reasonable solve speeds, approximately 100 Hz for NMPC and 400 Hz for LMPC. Though our examples are in 2D, it can be easily extend to higher dimensions [29]. Performance and speed were verified in both simulation and hardware during the competition, which ultimately helped us win RoboCup 2024 by a wide margin.

REFERENCES

- [1] G. I. Fernandez *et al.*, “Robocup 2024 adult-sized humanoid champions guide for hardware, vision, & strategy,” in *Robot World Cup*. Springer, 2024.
- [2] S. Raza and S. Haider, “Path planning in robocup soccer simulation 3d using evolutionary artificial neural network,” in *Advances in Swarm Intelligence: 4th International Conference, ICSI 2013, Harbin, China, June 12-15, 2013, Proceedings, Part II 4*. Springer, 2013, pp. 342–350.
- [3] R. Reinhart, T. Dang, E. Hand, C. Papachristos, and K. Alexis, “Learning-based path planning for autonomous exploration of subterranean environments,” in *2020 IEEE International Conference on Robotics and Automation (ICRA)*. IEEE, 2020, pp. 1215–1221.
- [4] G. Kulathunga, “A reinforcement learning based path planning approach in 3d environment,” *Procedia Computer Science*, vol. 212, pp. 152–160, 2022.
- [5] M. Popović, J. Ott, J. Rückin, and M. J. Kochenderfer, “Learning-based methods for adaptive informative path planning,” *Robotics and Autonomous Systems*, p. 104727, 2024.
- [6] A. Britzelmeier, A. De Marchi, and R. Richter, “Dynamic and non-linear programming for trajectory planning,” *IEEE Control Systems Letters*, vol. 7, pp. 2569–2574, 2023.
- [7] Y. Zhang, H. Sun, R. Chai, D. Kang, S. Li, and L. Li, “Optimal vehicle trajectory planning for static obstacle avoidance using nonlinear optimization,” *arXiv preprint arXiv:2307.09466*, 2023.
- [8] D. Pardo, L. Möller, M. Neunert, A. W. Winkler, and J. Buchli, “Evaluating direct transcription and nonlinear optimization methods for robot motion planning,” *IEEE Robotics and Automation Letters*, vol. 1, no. 2, pp. 946–953, 2016.
- [9] A. D. Ames, X. Xu, J. W. Grizzle, and P. Tabuada, “Control barrier function based quadratic programs for safety critical systems,” *IEEE Transactions on Automatic Control*, vol. 62, no. 8, pp. 3861–3876, 2016.
- [10] K. Garg and D. Panagou, “Control-lyapunov and control-barrier functions based quadratic program for spatio-temporal specifications,” in *2019 IEEE 58th Conference on Decision and Control (CDC)*. IEEE, 2019, pp. 1422–1429.
- [11] A. Agrawal and K. Sreenath, “Discrete control barrier functions for safety-critical control of discrete systems with application to bipedal robot navigation,” in *Robotics: Science and Systems*, vol. 13. Cambridge, MA, USA, 2017, pp. 1–10.
- [12] A. Manjunath and Q. Nguyen, “Safe and robust motion planning for dynamic robotics via control barrier functions,” in *2021 60th IEEE Conference on Decision and Control (CDC)*. IEEE, 2021, pp. 2122–2128.
- [13] M. Tayal, R. Singh, J. Keshavan, and S. Kolathaya, “Control barrier functions in dynamic uavs for kinematic obstacle avoidance: A collision cone approach,” in *2024 American Control Conference (ACC)*. IEEE, 2024, pp. 3722–3727.
- [14] M. Tayal and S. Kolathaya, “Polygonal cone control barrier functions (polyc2bf) for safe navigation in cluttered environments,” in *2024 European Control Conference (ECC)*. IEEE, 2024, pp. 2212–2217.
- [15] Y. K. Hwang, N. Ahuja *et al.*, “A potential field approach to path planning,” *IEEE transactions on robotics and automation*, vol. 8, no. 1, pp. 23–32, 1992.
- [16] J. Barraquand, B. Langlois, and J.-C. Latombe, “Numerical potential field techniques for robot path planning,” *IEEE transactions on systems, man, and cybernetics*, vol. 22, no. 2, pp. 224–241, 1992.
- [17] Y. Wang and G. S. Chirikjian, “A new potential field method for robot path planning,” in *Proceedings 2000 ICRA. Millennium Conference. IEEE International Conference on Robotics and Automation. Symposia Proceedings (Cat. No. 00CH37065)*, vol. 2. IEEE, 2000, pp. 977–982.
- [18] F. Bounini, D. Gingras, H. Pollart, and D. Gruyer, “Modified artificial potential field method for online path planning applications,” in *2017 IEEE Intelligent Vehicles Symposium (IV)*. IEEE, 2017, pp. 180–185.
- [19] Z. Wu, J. Dai, B. Jiang, and H. R. Karimi, “Robot path planning based on artificial potential field with deterministic annealing,” *ISA transactions*, vol. 138, pp. 74–87, 2023.
- [20] J. Liu, C. E. Adu, L. Lymburner, V. Kaushik, L. Trang, and R. Vasudevan, “Radius: Risk-aware, real-time, reachability-based motion planning,” *arXiv preprint arXiv:2302.07933*, 2023.
- [21] N. Malone, K. Lesser, M. Oishi, and L. Tapia, “Stochastic reachability based motion planning for multiple moving obstacle avoidance,” in *Proceedings of the 17th international conference on Hybrid systems: computation and control*, 2014, pp. 51–60.
- [22] T. Marcucci, M. Petersen, D. von Wrangel, and R. Tedrake, “Motion planning around obstacles with convex optimization,” *Science robotics*, vol. 8, no. 84, p. eadf7843, 2023.
- [23] T. Marcucci, J. Umenberger, P. Parrilo, and R. Tedrake, “Shortest paths in graphs of convex sets,” *SIAM Journal on Optimization*, vol. 34, no. 1, pp. 507–532, 2024.
- [24] S. M. LaValle and J. J. Kuffner Jr, “Randomized kinodynamic planning,” *The international journal of robotics research*, vol. 20, no. 5, pp. 378–400, 2001.
- [25] X. Wang, Z. Liang, L. Jiao, and Y. Fu, “Path planning of soccer robot based on improved heuristic rrt* algorithm,” in *2022 China Automation Congress (CAC)*. IEEE, 2022, pp. 810–815.
- [26] S. Jaiswal and S. Soumya, “Low-cost path planning in 2d environment using a* algorithm by considering slope of the obstacle,” *IFAC-PapersOnLine*, vol. 55, no. 1, pp. 783–788, 2022.
- [27] R. Steffens, M. Nieuwenhuisen, and S. Behnke, “Multiresolution path planning in dynamic environments for the standard platform league,” in *Proceedings of 5th Workshop on Humanoid Soccer Robots at Humanoids*, vol. 1, no. 2.3, 2010, p. 1.
- [28] W. Lee, G.-H. Choi, and T.-w. Kim, “Visibility graph-based path-planning algorithm with quadtree representation,” *Applied Ocean Research*, vol. 117, p. 102887, 2021.
- [29] T. Lozano-Pérez and M. A. Wesley, “An algorithm for planning collision-free paths among polyhedral obstacles,” *Communications of the ACM*, vol. 22, no. 10, pp. 560–570, 1979.
- [30] H. Rohnert, “Shortest paths in the plane with convex polygonal obstacles,” *Information Processing Letters*, vol. 23, no. 2, pp. 71–76, 1986.
- [31] Y.-H. Liu and S. Arimoto, “Finding the shortest path of a disc among polygonal obstacles using a radius-independent graph,” *IEEE Transactions on Robotics and Automation*, vol. 11, no. 5, pp. 682–691, 1995.
- [32] H.-P. Huang and S.-Y. Chung, “Dynamic visibility graph for path planning,” in *2004 IEEE/RSJ International Conference on Intelligent Robots and Systems (IROS)(IEEE Cat. No. 04CH37566)*, vol. 3. IEEE, 2004, pp. 2813–2818.
- [33] M. Kamel, M. Burri, and R. Siegwart, “Linear vs nonlinear mpc for trajectory tracking applied to rotary wing micro aerial vehicles,” *IFAC-PapersOnLine*, vol. 50, no. 1, pp. 3463–3469, 2017.
- [34] R. W. Brockett *et al.*, “Asymptotic stability and feedback stabilization,” *Differential geometric control theory*, vol. 27, no. 1, pp. 181–191, 1983.
- [35] I. Maurović, M. Baotić, and I. Petrović, “Explicit model predictive control for trajectory tracking with mobile robots,” in *2011 IEEE/ASME International Conference on Advanced Intelligent Mechatronics (AIM)*. IEEE, 2011, pp. 712–717.
- [36] J. Zhang, D. Wei, R. Gao, and Z. Xia, “A trajectory tracking and obstacle avoidance approach for nonholonomic mobile robots based on model predictive control,” in *2020 IEEE 16th International Conference on Control & Automation (ICCA)*. IEEE, 2020, pp. 1038–1043.
- [37] C. W. Warren, “Fast path planning using modified a* method,” in *[1993] Proceedings IEEE International Conference on Robotics and Automation*. IEEE, 1993, pp. 662–667.
- [38] M. Noto and H. Sato, “A method for the shortest path search by extended dijkstra algorithm,” in *Smc 2000 conference proceedings. 2000 IEEE international conference on systems, man and cybernetics. cybernetics evolving to systems, humans, organizations, and their complex interactions (cat. no. 0, vol. 3)*. IEEE, 2000, pp. 2316–2320.
- [39] H. I. Kang, B. Lee, and K. Kim, “Path planning algorithm using the particle swarm optimization and the improved dijkstra algorithm,” in *2008 IEEE Pacific-Asia Workshop on Computational Intelligence and Industrial Application*, vol. 2. IEEE, 2008, pp. 1002–1004.
- [40] A. B. Philpott, “Continuous-time shortest path problems and linear programming,” *SIAM journal on control and optimization*, vol. 32, no. 2, pp. 538–552, 1994.
- [41] R. Hou, M. Zhu, H. Nam, G. Fernandez, and D. Hong, “Fast and robust localization for humanoid soccer robot via iterative landmark matching,” in *2025 IEEE/RSJ International Conference on Intelligent Robots and Systems*. (Under Review).